Chinese Chemical Letters 34 (2023) 108515

Contents lists available at ScienceDirect

Chinese Chemical Letters

journal homepage: www.elsevier.com/locate/cclet

Recent advances of Rh-based intermetallic nanomaterials for catalytic applications

Lijie Zhu[a], Chunhai Li[a], Qinbai Yun[b], Sumei Han[c], Yong Lv[a,*], Qipeng Lu[c,d,e,*], Junze Chen[f,*]

[a] School of Instrument Science and Opto-Electronics Engineering, Beijing Information Science and Technology University, Beijing 100192, China
[b] Department of Chemistry, City University of Hong Kong, Hong Kong, China
[c] School of Materials Science and Engineering, University of Science and Technology Beijing, Beijing 100083, China
[d] Shunde Innovation School, University of Science and Technology Beijing, Foshan 528399, China
[e] Zhongguancun Institute of Human Settlements Engineering and Materials, Beijing 100083, China
[f] College of Materials Science and Engineering, Sichuan University, Chengdu 610065, China

ARTICLE INFO

Article history:
Received 17 January 2023
Revised 22 April 2023
Accepted 25 April 2023
Available online 28 April 2023

Keywords:
Rhodium
Intermetallics
Heterogeneous catalysis
Electrocatalysis

ABSTRACT

Rhodium (Rh) has received widespread attention in fundamental catalytic research and numerous industrial catalytic applications. Compared to homogeneous catalysts, Rh-based nanomaterials as heterogeneous catalysts are much easier to separate and collect after usage, making them more suitable for commercial use. To this purpose, there has been a constant demand in constructing stable and highly active Rh-based nanomaterials. In contrast to Rh-based solid solutions with a random distribution of metallic atoms in the lattice, Rh-based intermetallic compounds (IMCs) with a fixed stoichiometric ratio and an ordered atomic arrangement can ensure the homogenous distribution of active sites and structural stability in the catalytic process. In this review, we concentrate on the fabrication of Rh-based IMCs for catalytic applications. Various synthetic methods and protocols for the controlled preparation of Rh-based IMC are illustrated. Meanwhile, the catalytic applications and corresponding catalytic mechanisms are discussed. In addition, personal perspectives about the remaining challenges and prospects in this field are provided. We believe this review will be useful in directing the development of Rh-based IMC catalysts for heterogeneous catalysis.

1. Introduction

The platinum group metals contain six elements, including ruthenium (Ru), rhodium (Rh), palladium (Pd), osmium (Os), iridium (Ir), and platinum (Pt), which all possess high melting points, high heat and corrosion resistance [1]. Among these metals, Rh is one of the rarest and most expensive metals [2]. Because its 4d orbital is partially filled, Rh shows the suitable adsorption capacity of the reactants and hence improves the formation of key intermediates and ideal final products [3]. Till now, Rh-based materials have been demonstrated to be the optimal catalysts for a multiplicity of heterogeneous catalysis, including selective hydrogenation [4–12], alcohol oxidation [13–21], hydrogen evolution reaction (HER) [22–28] and hydrogen oxidation reaction (HOR) [29–31]. In order to reduce the prohibitive cost and improve the catalytic performance of the Rh-based catalysts, the researchers have developed advanced synthetic strategies to incorporate Rh with the secondary metals and thus prepare solid solutions and intermetallic compounds (IMCs) [30,32-36]. With the assistance of the ensemble/electronic/geometrical effects, the adsorption/desorption properties and the catalytic performance could be further improved [37–40].

Compared to the solid solutions with a random distribution of metallic atoms in the lattice, IMCs with fixed stoichiometric ratios and ordered atomic arrangement can guarantee the homogeneous distribution of active sites [40–44]. Meanwhile, the stronger metallic bond and enhanced interaction between Rh and secondary metals, *e.g.*, Sb, Ga, In, Zn, Sn, Ge, Bi, Pb, can significantly enhance the structural stability and electronic effects, which further improve the catalytic performance, especially in both of activity and durability aspects [4,45-48]. Significantly, for selective hydrogenation, the isolated active sites with geometric constraints could effectively limit the over-hydrogenation reaction, thus improving the selectivity for certain products [45,46]. Therefore, in the past few

* Corresponding authors.
E-mail addresses: lvyong@bistu.edu.cn (Y. Lv), qipeng@ustb.edu.cn (Q. Lu), jzchen@scu.edu.cn (J. Chen).

https://doi.org/10.1016/j.cclet.2023.108515
1001-8417/

years, tremendous endeavors have been dedicated to preparing Rh-based IMCs for high performance catalysis.

In this review, we focus on the recent progress in the preparation and catalytic applications of Rh-based IMCs. And the review is organized into three parts. In the first part, the preparation strategies and specific synthetic protocols of Rh-based IMCs are comprehensively introduced. In the second part, the catalytic applications based on Rh-based IMCs, including semihydrogenation of acetylene, hydroformylation, chemoselective hydrogenation of nitroarenesare, electrocatalytic alcohol oxidation, electrocatalytic hydrogen evolution, hydrogen oxidation, are illustrated systematically, especially for the related catalytic enhancement mechanisms. In the final part, the future opportunities and challenges in this promising research area are deliberated.

2. Preparation and characterization of Rh-based imc nanomaterials

Bulk IMCs are typically prepared through synthetic techniques involving high temperatures, including powder metallurgy, induction heating, and vacuum arc melting [38,43,49]. The successful preparation of IMCs depends on the thermal diffusion equilibration of different metal atoms at high temperature. However, for these methods, it is tough to get nanosized IMCs with uniform size distribution, even incorporated with the post-treatments, *e.g.*, sonication and ball milling exfoliation. On the other hand, the annealing of solid solution nanoparticles or core-shell nanostructure can facilitate the disorder to order transition [50]. But the high temperature will induce the overgrowth of nanocrystals and aggregation of particles, leading to the uncontrollable growth of large particles with limited specific surface area.

With the rapid development of preparation technologies and corresponding theories in nanomaterials, researchers have explored more effective methods to obtain IMC nanomaterials with controlled particle sizes. Meanwhile, the corresponding formation mechanisms of IMC nanomaterials have been investigated [38,51-53]. Up to now, two major strategies for the preparation of Rh-based IMC nanocrystals are proposed based on the published results: (1) wet chemical synthetic method in the solution phase; (2) substrate-anchored or confined thermal annealing method under an inert or reducing atmosphere. In the following sections, we will introduce the key factors for the formation of IMCs, summarize the recent achievements in preparation of Rh-based IMC nanomaterials and highlight the corresponding formation mechanism. Meanwhile, some characterization techniques will be introduced.

2.1. Key factors for the formation of IMCs

Thermodynamic and kinetic analyses indicate that the formation of IMC nanocrystals is regulated by several factors, including surface free energy, activation barrier, and diffusion barrier [43]. These factors can be influenced by various parameters, such as chemical composition, crystal structure, size and shape of IMC nanomaterials, and corresponding reaction conditions.

Chemical composition and crystal structure: The formation of IMCs depends on the chemical composition, and intermetallic phases are only favored in a limited number of bimetallic systems [52]. Therefore, screening phase diagrams is necessary to identify the candidate metal pairs for IMCs. Additionally, a sufficient difference in electronegativity is crucial for the formation of IMCs, as it can contribute to covalent bonding and reduce the miscibility of two components, thus favoring the formation of IMC phases [54]. Moreover, the difference in crystal structure between disordered and ordered phases is vital to the phase transition. The disorder-to-order transitions between two similar crystal structures are easier due to the lower energy barrier and larger driving force, whereas phase transitions between two phases with large structural differences require overcoming a higher energy barrier [43].

Size and shape: Reducing the size of a crystal to a few nanometers results in an increase in surface free energy, which leads to a rapid decrease in the disorder-to-order transition temperature. Smaller nanocrystals facilitate faster atom diffusion in the phase transition process. Theoretically, the required driving force to an ordered phase could be reduced [55]. Additionally, the shape of the nanocrystal plays an important role in determining the total change in Gibbs' free energy. As the specific surface free energy of distinct facets is different, modulating the exposed facets can also influence the disorder-to-order transition temperature [41].

Reaction conditions: The formation of IMCs can also be influenced by chemical reaction conditions. High reaction temperatures or pressures can provide sufficient energy to overcome the high diffusion barrier required for the rearrangement of metal atoms, resulting in the formation of IMCs with ordered structure. Furthermore, long-term heating and annealing are usually required to ensure the complete disorder-to-order phase transition [56].

2.2. Wet chemical *synthesis*

The wet-chemical method is a convenient and powerful technology for synthesizing noble metal nanomaterials [57]. By employing the specific capping ligand and reducing agent, the reduction rate of metal ions, nucleation and growth behaviors can be manipulated [58–60]. Therefore, noble metal nanomaterials with rationally designed chemical composition, favored particle size and morphology could be synthesized. To obtain noble metal-based IMCs with an atomically ordered structure, these key parameters of nanomaterials, including chemical composition, size, and morphology, are vital for the disorder-to-order transition in atomic scale [50,61].

For the different compositions of IMCs, the bond strength is highly associated with the melting point of the materials and the diffusion rate of atoms [43]. Because the heating temperature of the wet-chemical synthesis is usually below 350 °C, this method has certain limitations and is appropriate for obtaining Rh-based IMC nanocrystals containing low melting-point metals, *e.g.*, Bi (271.5 °C), Pb (327.46 °C), and Sb (630.63 °C) [62,63]. For example, Xiaoqing Huang's group developed a hydrothermal method to synthesize Rh_2Sb nanocrystals with multiple nanobranches (named as Rh_2Sb NBs, Fig. 1a) at 200 °C for 3 h, in which $Rh(acac)_3$ and $SbCl_3$ served as the metal precursors, benzyl alcohol as the solvent and polyvinyl pyrrolidone as the surfactant [64]. The high-magnification transmission electron microscopy (TEM) image (Fig. 1b) demonstrated the branched nature of Rh_2Sb with 88.5 nm in average length and 4.2 nm in average diameter. Notably, the time-dependent control experiments revealed that the length of NBs is increasing along with prolonging the reaction time, indicating the formed NB is an integrated structure rather than assembled by nanorods as building blocks. From the aberration-corrected high-resolution TEM (AC-HRTEM) image (Fig. 1c) and structure analysis (XRD pattern in Fig. 1d), Rh_2Sb NBs crystallize in the orthorhombic structure (*Pnma* space group), and the growth direction of NBs is along ⟨001⟩ direction. The most exposed facet is the high-index {210} facet, on which the Rh atoms are ordered and isolated by Sb atoms. X-ray absorption fine structure (XAFS) spectroscopy analysis (Fig. 1e) indicated that the Rh in Rh_2Sb NBs is in the metallic state. And the Fourier-transformed extended X-ray absorption fine structure (FT-EXAFS, Fig. 1f) demonstrated that there are no Rh-Rh characteristic peaks formed and Rh atoms are isolated. This example demonstrated that the wet chemical method is beneficial for controlling the morphology and preventing the aggregation of Rh-based IMC nanocrystals.

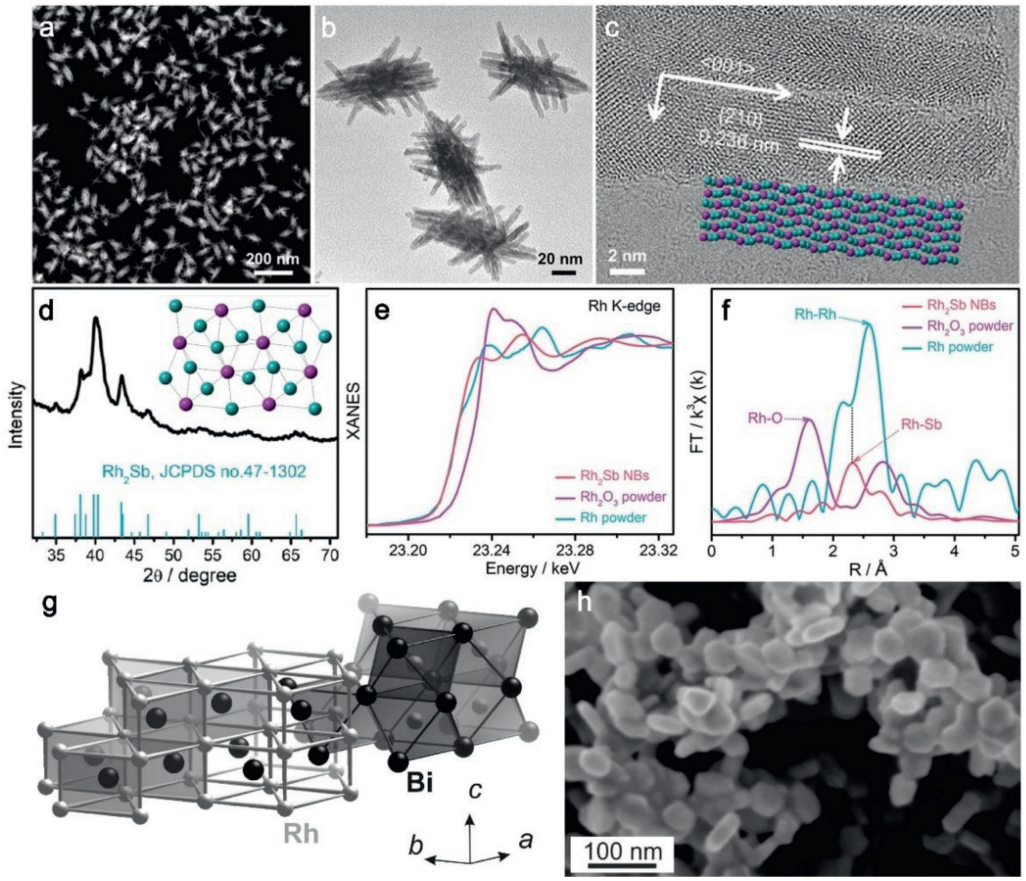

Fig. 1. (a) High-angle annular dark-field scanning transmission electron microscopy (HAADF-STEM) image and (b) TEM image of Rh_2Sb NBs. (c) HRTEM image and atomic mode of Rh_2Sb with exposed {210} facet. (d) PXRD pattern of Rh_2Sb NBs. Inset: Crystal structure of Rh_2Sb along [010] plane. The purple and cyan spheres represent Sb and Rh atoms, respectively. Normalized Rh K-edge (e) X-ray absorption near edge structure (XANES) and (f) EXAFS spectra of Rh_2Sb NBs, Rh_2O_3 powder, and Rh powder. Reproduced with permission [64]. Copyright 2021, Wiley-VCH. (g) Crystal structure of RhBi (NiAs type of structure). (h) Scanning electron microscopy (SEM) image of RhBi nanoplates. Reproduced with permission [67]. Copyright 2012, American Chemical Society.

Compared to traditional heating methods, microwave radiation is more efficient. It has been widely used in heating high polarity solvents owing to the unique heating mechanism inside the reaction vessels [47,65,66]. Michael Ruck group and Marc Armbrüster group employed this method and prepared a series of Rh based IMC nanocrystals, including RhSb, $RhPb_2$, and RhBi [67,68]. During the microwave-assisted polyol reduction, ethylene glycol was employed as both solvent and reducing agent. Meanwhile, to tune the reducibility of the metal precursors, KOH was added to the solution to modify the pH value. The obtained RhBi IMCs displayed pseudohexagonal plates with a diameter of 60 nm and high crystallinity (NiAs type of structure, Figs. 1g and h) [67]. In Rh–Sb and Rh–Pb systems, many kinds of IMCs have thermal stable crystal structures but different stoichiometric ratios. However, their experimental results demonstrated that simple control of the initial ratio between different metal precursors is hard to tune the stoichiometry and corresponding crystal structure. The morphology of the obtained RhSb IMCs is star-shaped agglomerates, while $RhPb_2$ is a non-uniform nanoparticle. Because of the fast reduction rate of Rh(II) compared to the other elements (*i.e.*, Sb, Pb, and Bi), the obtained Rh-based IMC nanocrystals always possess small particle sizes and weak diffraction signals [68].

The ordered atomic structure of IMCs is an ideal model for improving the catalytic activity and stability on account of the negative formation enthalpy as well as the strong interaction between different elements. Combining the benefits of IMCs and high entropy alloys, Quan and coauthors developed a convenient wet chemical method and synthesized *hcp* high-entropy PtRhBiSnSb IMC nanoplates based on the identical *hcp* structures of PtBi, PtSn, PtSb and RhBi IMCs (Figs. 2a and b) [69]. The AC-HAADF-STEM (Fig. 2c) and the simulated model (Figs. 2d-h) demonstrated that the substitution of Rh atoms on Pt columns, and the substitution of Sn/Sb atoms on Bi columns in the obtained high-entropy (PtRh)(BiSnSb) IMC. The lattice spacing of the (100) planes is ~0.361 nm, which is larger than those of (100) planes in PtSn (*i.e.*, 0.355 nm) and PtSb (*i.e.*, 0.358 nm) IMCs and small than that of (100) plane in PtBi (0.374 nm) IMC (Fig. 2c). The 2D Gaussian fitting of the intensities and positions of different atoms in AC-HAADF-STEM image demonstrate the intensity variation clearly, which are all consistent with the simulated models (Figs. 2e-h). Therefore, the atomic configuration and atomic structure of *hcp* (PtRh)(BiSnSb) can be identified.

The above examples demonstrated that the wet-chemical methods have many advantages in optimizing the chemical composition and tuning the morphology of Rh-based IMCs. In the near future, more effective and practical recipes should be developed for achieving high-performance Rh-based IMC catalysts.

2.3. Thermal annealing method

Based on the kinetic and thermodynamic analyses, the solid solution with a disordered structure possesses a metastable structure in contrast to the IMC phase when the preparation temperature is below the disorder-to-order transition temperature [70]. Theoretically, if the solid solution nanocrystals are heated at a high temperature for enough time, they could be converted to IMCs based

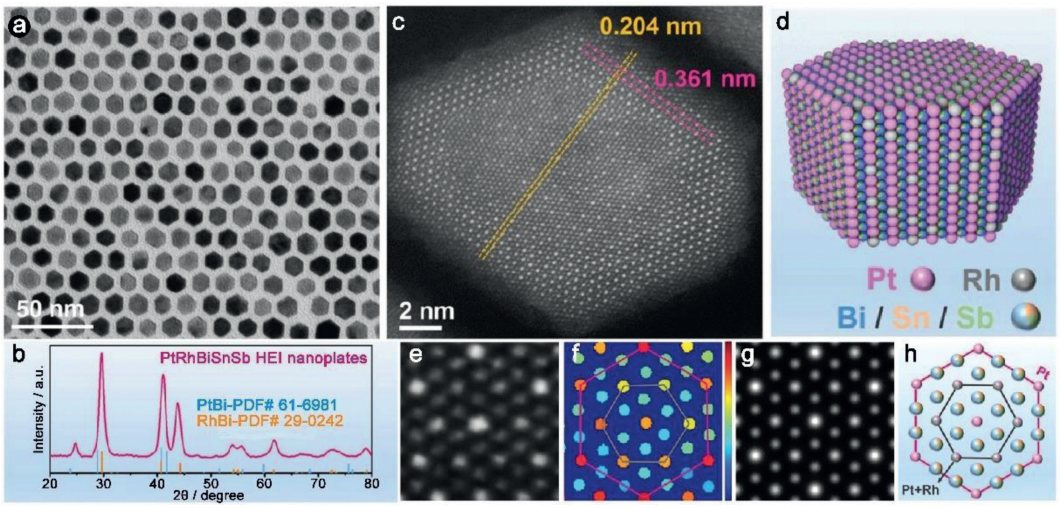

Fig. 2. (a) TEM image, (b) XRD pattern, and (c) AC-HAADF-STEM image of high-entropy PtRhBiSnSb IMC nanoplates. (d) Schematic model of the atomic arrangement in a high-entropy PtRhBiSnSb IMC nanoplate. (e) AC-HAADF-STEM image of the typical Rh-substituted Pt columns and (f) the corresponding color dots. (g) Simulated image and (h) atomic model of the Rh-substituted Pt columns. Reproduced with permission [69]. Copyright 2022, Wiley-VCH.

on the phase diagram [56]. By using this strategy, lots of Rh-based IMCs could be prepared. For example, the Zhong group employed the arc-melting method and prepared ternary $Ir_{1-x}Rh_xSb$ by mixing powders containing metallic Ir, Rh, and Sb as raw materials [71]. However, it is undeniable that this method is hard to control the particle size, uniformity, and morphology.

Compared with the arc-melting method, the impregnation method is simple and effectively to deposit IMC nanocrystals on the substrate [5,6,45,72-74]. Meanwhile, the size distribution and dispersity can be controlled. Komatsu group developed a general impregnation method to prepare Rh-based IMC nanocrystals on SiO_2 gel as the substrate. The obtained Rh-based IMC nanocrystals include cubic *Pm*$\bar{3}$*m* (RhZn, RhGa, and RhIn), orthorhombic *Pnma* (RhSb and RhGe), hexagonal *P6/mmm* (RhPb), cubic $P2_13$ (RhSn); hexagonal $P6_3/mmc$ (Rh_3Pb_2 and RhBi) and tetragonal *I4/mcm* ($RhPb_2$) (Fig. 3a) [45]. The preparation procedure could be divided into two steps. In the first step, the silica-supported Rh (*i.e.*, Rh/SiO_2) catalysts were obtained *via* a pore-filling impregnation method, in which the $Rh(NO_3)_3$ as precursor was mixed with the dried silica gel. After drying at 100 °C, the powder was calcined under dry air at 450 °C for 4 h followed by reduced under H_2 flow for 2 h at 550 °C. In the second step, the Rh-based IMCs were added into the aqueous metal precursor solutions, *e.g.*, $SbCl_3$, $Ga(NO_3)_3$, $(NH_4)_2GeF_6$, $InCl_3$, $Pb(NO_3)_2$ and $Zn(NO_3)_2$, according to the certain stoichiometric ratio. After dried on the hotplate, the mixed powders were reduced under the H_2 atmosphere at 800 °C for 1 h. Finally, the Rh-based IMC nanocrystals on the SiO_2 substrate could be obtained. Taking obtained RhBi nanoparticles (average size ~4.1 nm, Figs. 3b and c) as an example, a series of characterizations, including HRTEM (Figs. 3d and e) and elemental mapping (Figs. 3f-i), demonstrated that the formed nanoparticles are single crystals with ordered IMC structure [46,75].

In order to get Rh-based IMC nanocrystals with smaller size distribution to expose more active sites, Haiwei Liang group developed a facile strategy to prepare a library of Rh-based IMC nanocrystals on sulfur-doped carbon substrate based on the conventional impregnation method [48]. By employing the strong interaction between metal and sulfur, the Rh-based IMC nanocrystals can be firmly anchored on the substrate. Meanwhile, the overgrowth can be suppressed during the sintering up to 1000 °C. By employing this strategy, 10 kinds of Rh-based IMCs with sub-5-nm were obtained, including *Pm*$\bar{3}$*m* (Rh_3Ti, RhIn, RhFe, RhGa, Rh_3V), *Pnam* (RhSb, Rh_2Sb, RhGe, Rh_2Ge), and *P63/mmc* (Rh_3Sn_2). In the synthetic process, $RhCl_3$ as the Rh precursor and the other metal salts with certain stoichiometric ratios were employed for preparing these IMCs except Rh_3Ti and Rh_3V. Because the Ti and V elements tend to form metal oxides, excess Ti and V precursors were used to ensure the formation of pure IMC phases. Taking obtained RhGa IMC nanocrystals as an example, the XRD pattern (Fig. 4a) indicates that the obtained RuGa IMCs belong to CsCl type structure, and the average particle size is 1.95 nm based on the calculation from the low magnification TEM image (Figs. 4b and c). According to the HAADF-STEM images (Figs. 4d and e), the periodic square arrays are observed, in which one Rh atom is located in the center, and four Ga atoms are located around the Rh atom. The corresponding FFT pattern exhibits a series of characteristic diffraction spots, which is attributed to the CsCl type structure along the [001] direction (Figs. 4f and g). In order to investigate the effects of metal-S interaction on the size control of Rh-based IMCs, they also prepared RhIn, RhGa, and RhFe IMCs on two kinds of commercial carbon supports without sulfur doping. According to the XRD results, the obtained products with much sharper diffraction peaks possess large particle sizes, which demonstrated that suppressing the sintering is highly associated with the metal-sulfur interaction [48].

To improve stability and durability, IMC nanocrystals can also be deposited into the nanopores or channels of the substrate [76,77]. For example, Huang group developed an incipient wetness impregnation method and synthesized a list of Rh-based IMC nanocrystals on mesoporous silica (*i.e.*, SBA-15), including RhZn, Rh_3Sn_2, RhSb, RhIn, RhGa, and RhBi. The low magnification TEM image of the prepared RhZn/SBA-15 demonstrated that RhZn nanoparticles with high monodispersity are distributed within the channel of the SBA-15 framework (Fig. 4h). The average particle size of RhZn IMC nanocrystals is 9.6 ± 0.6 nm, which is well matched with the calculated grain size of 9.2 nm from the XRD pattern according to the Scherrer equation. AC-HAADF-STEM images show the ordered arrangement of Zn and Rh atoms throughout a nanocrystal (Figs. 4i-k) [4].

The thermal annealing method is facile and effective to promote the formation of the ordered structure. With the assistance of the anchoring and confinement effects from certain substrates, the crystal size and dispersity of Rh-based IMC nanocrystals can be well controlled [77,78]. It is hopeful that this method can be extended to prepare more kinds of Rh-based IMC composite catalysts in large scale.

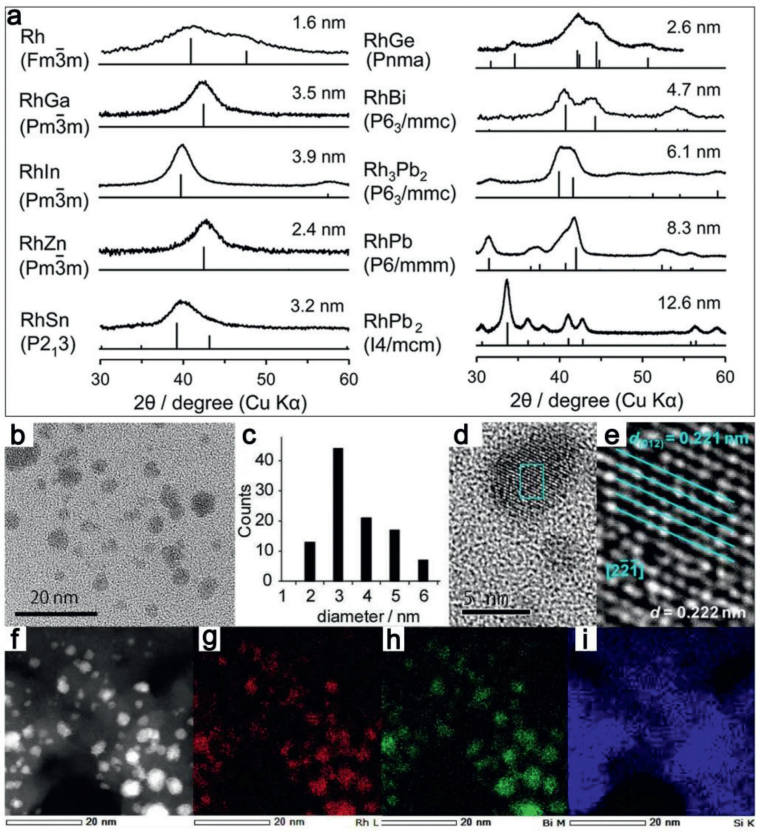

Fig. 3. (a) XRD patterns of Rh-based IMC nanocrystals on the SiO_2 substrate and reference data (ICDD-PDF). The crystallite sizes are calculated by using the Scherrer equation. Reproduced with permission [45]. Copyright 2016, The Royal Society of Chemistry. (b) TEM image and (c) the corresponding size distribution of RhBi IMC nanoparticles. (d) HRTEM image of a typical RhBi IMC nanoparticle. (e) The magnified image of the blue square region in (d). (f-i) HAADF-STEM image of RhBi IMC nanoparticles and the corresponding EDX elemental mapping images. Reproduced with permission [46]. Copyright 2017, American Chemical Society.

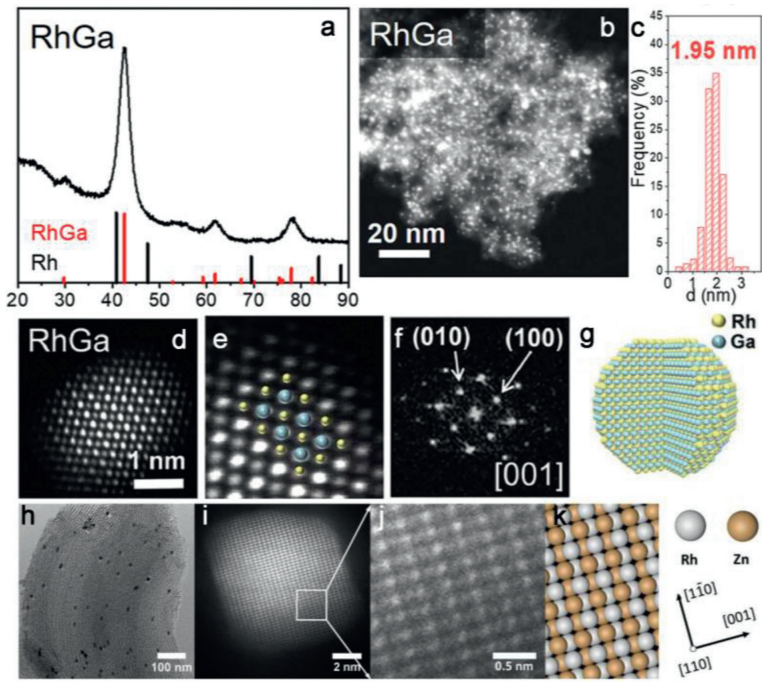

Fig. 4. (a) XRD pattern, (b) HAADF-STEM image, and (c) corresponding size distribution of RhGa IMC nanoparticles on a sulfur-doped carbon substrate. (d, e) AC-HAADF-STEM images, (f) the corresponding FFT pattern of a typical RhGa IMC nanoparticle. (g) The crystal structure model of RhGa IMC (*i.e.*, CsCl structure type). Reproduced with permission [48]. Copyright 2022, American Chemical Society. (h) TEM of RhZn/SBA-15. (i) AC-HAADF-STEM image of an RhZn IMC particle. (j) Enlarged AC-HAADF-STEM image and (k) simulated model of the RhZn crystal structure. Reproduced with permission [4]. Copyright 2022, American Chemical Society.

2.4. Characterization techniques

Various characterization techniques can be employed to study the structure of IMCs, including XRD, selected area electron diffraction (SAED), and AC-HAADF-STEM. XRD is a commonly used technique to determine the crystal structure of IMCs. Compared to the solid solution, the presence of superlattice peaks in XRD patterns indicates the ordered arrangement of atoms. SAED patterns with concentric rings or spots can demonstrate the existence of characteristic lattice planes of IMCs. Compared with these diffraction analysis techniques, AC-HAADF-STEM can be used to directly observe the ordered structure at the atomic level. In the IMCs, different element atoms occupy well-defined positions in crystal lattice. Due to the atomic-number (Z)-sensitive nature of the HAADF-STEM contrast, the different kinds of atoms could be easily distinguished. In addition, thermal analysis techniques, such as differential scanning calorimetry (DSC) and thermogravimetric analysis (TGA), are also useful for studying the thermal stability and phase transitions of IMCs. These techniques provide valuable information about the thermal behavior and transition temperature of IMCs regarding their size/shape/chemical composition under various conditions.

3. Utilization of rh-based IMCs in catalytic reactions

The catalytic performance of solid-state catalysts is governed by the ensemble/electronic/geometrical structures of the active sites on the catalyst surface [79]. Compared with disordered alloys, IMCs with crystalline structure exhibit highly ordered atomic arrangement, which makes them attractive candidates as catalysts for selective hydrogenation and electrocatalytic reactions. Importantly, IMCs are generally more stable than disordered alloys during catalytic reactions. The Rh-based IMCs possess stronger metallic bonds and enhanced interactions between Rh and secondary atoms, resulting in more stable chemical and geometric structures. In the following parts, we will illustrate the utilization of Rh-based IMCs in some important catalytic reactions, including semihydrogenation of acetylene, hydroformylation, chemoselective hydrogenation of nitroarenes, alcohol oxidation, hydrogen evolution, and hydrogen oxidation [41].

3.1. Semihydrogenation of acetylene

Previous research results reveal that IMCs exhibit high catalytic activity and selectivity for the semihydrogenation of alkyne to alkene, which is one of the most significant and extensively research categories in the realms of fundamental and applied chemistry [80]. The key concern for these reactions is inhibiting the over-hydrogenation of alkyne to alkane. And the excess capability of hydrogen activation results in the undesired over-hydrogenation of alkyne. In general, the dilution of active metal sites on the catalyst surface brought on by forming an IMC phase results in lower activity for hydrogen dissociation [72]. Additionally, the highly ordered atom arrangement on the surface of IMC could provide a suitable reaction environment for selective catalytic reactions. Much effort has been devoted to developing IMC-based catalysts for semihydrogenation [81–84]. For example, Rh_mM_n (M = Ge, In, Bi, Sn, and Sb) supported on silica were prepared and examined as catalysts for the semihydrogenation of diphenylacetylene (DPA) to *trans*-stilbene (*trans*-ST) [72]. The overhydrogenation of DPA results in the formation of diphenylethane (DPE, Fig. 5a). Monometallic Rh catalyst shows high selectivity towards DPE. Interestingly, the over-hydrogenation could be inhibited by introducing second metals. Among the obtained IMC-based catalysts, Rh_2Sb showed full conversion of DPA with a significantly greater selectivity to *trans*-ST compared to monometallic Rh. RhSb possesses a moderate hydrogenation ability capable of half-hydrogenation but minimal over-hydrognation, leading to the selective isomerization of *cis*-stilbene (*cis*-ST, Fig. 5b). Rh-Rh sites on catalyst surfaces are diluted as a result of the creation of an IMC phase, which lowers the activity of hydrogen dissociation. The modest hydrogenation capacity of Rh_2Sb is the main reason for its highest *trans*-ST yield [72].

3.2. Hydroformylation

Hydroformylation of olefins and syngas to form aldehydes is an essential reaction in the chemical industry, which is traditionally catalyzed by homogeneous catalysts [85–87]. During the hydroformylation processes, the addition of the formyl group occurs at either side of the olefin double bonding, resulting in the formation of a mixture of branched and linear aldehydes. Organometallic Rh-based complexes with phosphine ligands display excellent performance in synthesizing the preferred linear aldehydes [88,89]. However, the limited recyclability constrains their applications. Recently, Huang *et al.* reported the synthesis of RhZn IMC nanoparticles supported on SBA-15, *i.e.*, mesoporous silica, as a highly efficient heterogeneous catalyst for the hydroformylation of styrene [4]. In their study, a series of Rh-based IMC catalysts, including RhZn, Rh_3Sn_2, RhIn, RhGa, and RhBi, is prepared by an incipient wetness impregnation method. Although most of the obtained IMC catalysts showed low aldehyde yields, RhIn and RhZn exhibited significantly higher selectivity for aldehyde. In particular, RhZn/SBA-15 displays exceptional catalytic activity and linear aldehyde selectivity with a remarkably high turnover frequency (TOF) of 3090 h^{-1}, which is roughly three times higher than that of the homogeneous Wilkinson's catalyst (Fig. 5c). Importantly, the yield of aldehydes and the linear to branch ratio (l:b) from RhZn (90.6% and l:b = 1.4) are much higher than both Wilkinson's catalyst (85.2% and 1:b = 1.3) and Rh/SBA-15 (17.3% and 1:b = 1.1). The relatively weak CO adsorption on the RhZn surface was validated by CO-DRIFTS investigations, demonstrating that more Rh active sites for C=C and H_2 adsorption and facilitating the production and desorption of product species, resulting in the increased hydroformylation activity (Fig. 5d). Additionally, the authors used DFT simulations to learn more about the mechanism of the regioselectivity of RhZn. According to the results, RhZn (110) has the highest activity that is expected to favor the branched product. In contrast, RhZn (111) has higher exposure but less activity that is likely to favor the linear product (Figs. 5e and f).

3.3. Chemoselective hydrogenation of nitroarenes

The selective reduction of nitroarenes is a vital reaction to obtain aminoarenes. Aniline and its derivatives are of great commercial importance in the fine chemical, agrochemical, and pharmaceutical industries [90,91]. The selective hydrogenation of the nitro group in the presence of other functional groups sensitive towards hydrogenation, such as olefin, aldehyde, cyano, and benzyl ether, is an important challenge in industrial processes [37]. By using gaseous hydrogen and monometallic transition metal catalysts, the selective hydrogenation of nitrostyrene to obtain aminostyrene reveals that the vinyl group is more amenable to hydrogenation than the nitro group [41]. Under mild reaction conditions, it is discovered that Rh-based IMCs are very active and highly selective catalysts for the hydrogenation of different nitroarenes [10,92]. For example, Furukawa *et al.* reported the preparation of a series of Rh-based IMCs on silica gel (named as Rh_xM_y/SiO_2, M = Sn, Fe, Bi, Ge, Ga, Ni, In, Sb, Pb, or Zn) and investigated their catalytic performance in reduction of nitroarenes [45]. Various nitroarenes containing cyano, carbonyl, or halo groups were selectively converted into the corresponding aminoarenes with

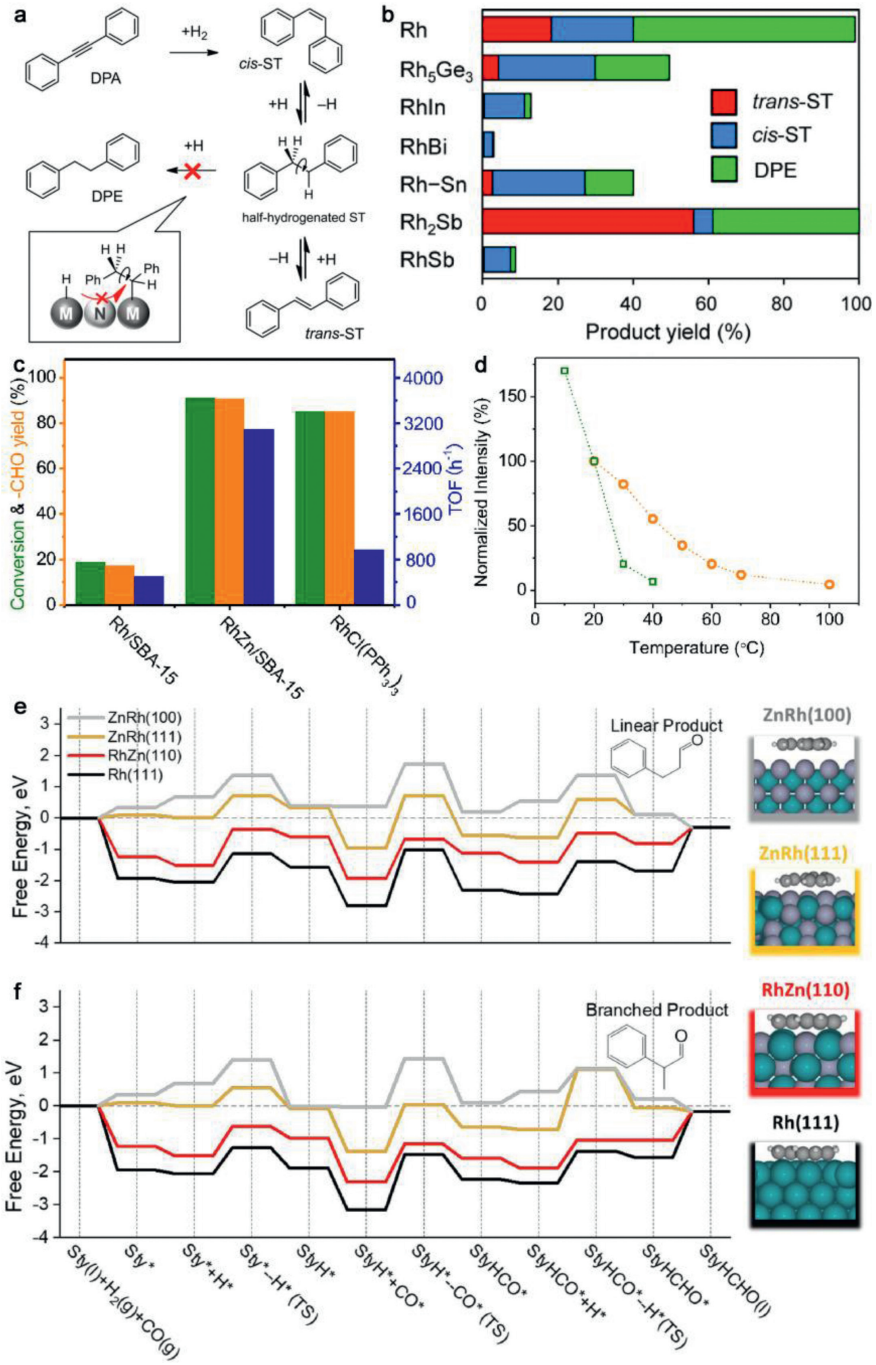

Fig. 5. (a) Synthesis of *trans*-ST from DPA in the presence of hydrogen: reaction routes and methodology. (b) Product yields in the hydrogenation of DPA using different Rh-based catalysts. Reproduced with permission [72]. Copyright 2014, American Chemical Society. (c) Comparison of the catalytic performance of $RhCl(PPh_3)_3$, RhZn/SBA15, and Rh/SBA-15 for the hydroformylation of styrene. (d) The strength evolution of CO adsorption peak with the temperature for RhZn/SBA-15 (green) and Rh/SBA-15 (orange). The most stable adsorption configurations of styrene on each surface are shown to the right (side view). The Rh, Zn, C and H atoms are represented by green, light purple, gray and white spheres, respectively. Free energy diagrams for styrene hydroformylation *via* the (e) linear and (f) branched product pathways at 100 °C and 1 atm on the surfaces of ZnRh (100), ZnRh (111), RhZn (110) and Rh (111). The right images are the most stable adsorption configurations of adsorbed styrene (side view) on the respective surfaces. Atom colors for adsorbed species: C (gray), H (white), Zn (light purple), and Rh (green). Reproduced with permission [4]. Copyright 2021, American Chemical Society.

high yields *via* $RhIn/SiO_2$. For the hydrogenation of 4-nitrostyrene, $RhIn/SiO_2$ showed the highest selectivity (97%) towards the desired product 4-aminostyene among the obtained Rh-based IMCs (Fig. 6a). By contrast, monometallic Rh showed 94% selectivity towards the undesired product 4-ethylnitrobenzene. It was found that the selectivity of various Rh-based IMC catalysts significantly depends on the type of functional group in nitrostyrene, nitro, or vinyl, which binds to the surface preferentially. The vinyl group prefers the side-on configuration because of the coadsorption of the phenyl moiety, in contrast, the nitro group can attach to the Rh atom in the end-on configuration. DFT calculations indicated that the Rh atom at concave and In atom at convex appear on the surface of the RhIn IMC catalyst, which can capture the nitro group with end-on configuration while effectively reducing the vinyl-π adsorption (Fig. 6b) [45]. Similarly, Yin *et al.* reported a general synthetic strategy for fabricating a series of ultrasmall (<4 nm) Rh-based IMC catalysts [48]. RhSb was used as a catalyst for the hydrogenation of *p*-chloronitrobenzene to produce *p*-chloroaniline.

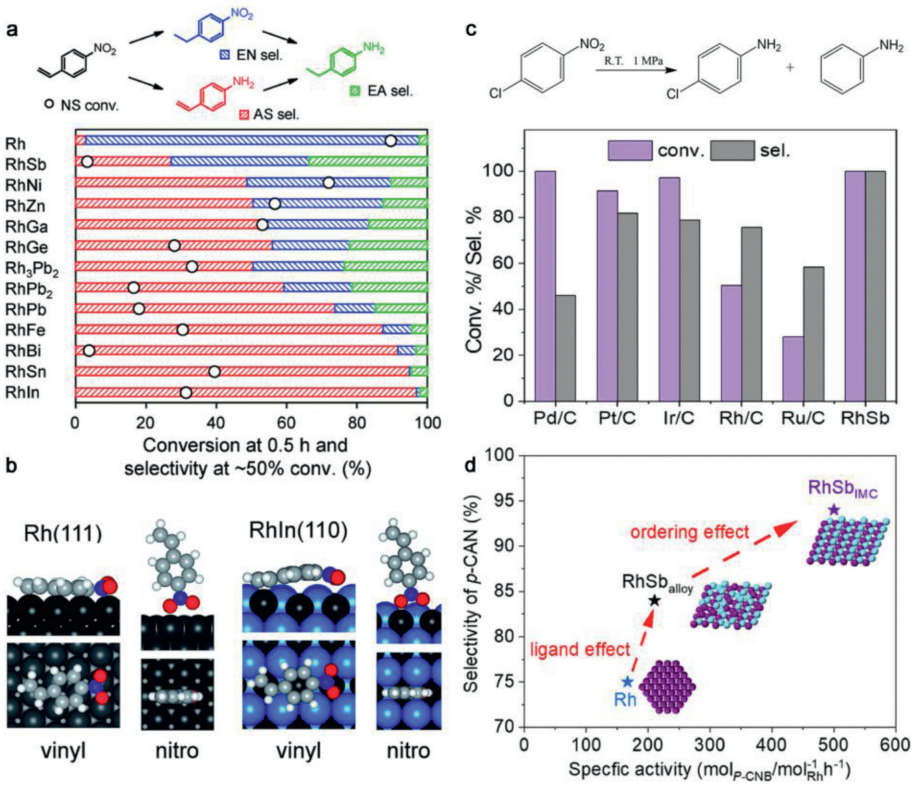

Fig. 6. (a) Product distribution and conversion in 4-nitrostyrene hydrogenation on different Rh-based alloys supported by SiO_2. (b) Optimized structure of 4-nitrostyrene adsorbed on Rh (111) facet and RhIn (110) facet with vinyl and nitro moieties. Views from the side (top), and top (bottom) are displayed. Reproduced with permission [45]. Copyright 2016, The Royal Society of Chemistry. (c) Catalytic performance of commercial monometallic catalysts and RhSb IMCs. (d) Specific activity and selectivity at 50% conversion, demonstrating the ligand and ordering effects in the ordered IMC structure. Reproduced with permission [48]. Copyright 2022, The Royal Society of Chemistry.

For comparison, commercial Ru/C, Pt/C, and Pd/C were also measured under the same reaction condition. Commercial catalysts had good activity (>93% conversion), however, they had low selectivity for *p*-chloroaniline due to the undesired over-hydrogenation. The over-hydrogenation was entirely stopped by the RhSb catalyst, which also achieved exceptional selectivity (>99%) for *p*-chloroaniline (Fig. 6c). Both activity and selectivity of RhSb were superior to those of monometallic Rh. From the point of view of structural analysis, the atomically ordered RhSb surface comprises 1D aligned Rh rows separated by Sb atoms with intermittent Rh exposure sites. The over-hydrogenation process is thought to be effectively constrained by the geometric limitations on the RhSb surface (Fig. 6d) [48].

Besides using gaseous hydrogen, other hydrogen sources such as methanol can also be used in the selective hydrogenation of nitro groups. The chemoselective hydrogenation of *p*-nitrostyrene to *p*-aminostyrene was investigated by using Rh-based IMCs. Interestingly, the increase in the electronegativity of the secondary metal in Rh-based IMCs created polar sites and boosted the activation of methanol as a hydrogen donor, which sped up the hydrogenation of the nitro group of *p*-nitrostyrene. As a result, the yield of *p*-aminostyrene could be increased. It is concluded that $RhPb_2$ IMC containing the Pb element with the most electronegative value in their study exhibited high selectivity toward *p*-aminostyrene and the highest conversion (94%) among the investigated Rh-based IMC catalysts [6].

3.4. Alcohol oxidation

Compared with hydrogen-oxygen fuel cells, direct alcohol fuel cells (DAFCs) have attracted more attention due to their high energy density and the avoidance of hidden safety hazards brought by hydrogen [93–97]. Recent studies have demonstrated that Rh-based IMCs have outstanding electrocatalytic activity toward oxidation processes at the anode in DAFCs [69,98-100]. For example, the incorporation of a small amount of Rh into high-entropy PtRhBiSnSb IMC nanoplate could significantly enhance the activity in methanol oxidation (MOR) in the alkaline electrolytes [69]. A record-high MOR activity of 19.529 A/mg_{Pt+Rh} was achieved as catalyzed by PtRhBiSnSb with 9.8 percent of Rh (Fig. 7a). The electrochemical durability of PtRhBiSnSb IMC nanoplates was evaluated by sweeping 5000 CV cycles in the electrolyte. As shown in Fig. 7b, after the cycle test, the current densities of PtRhBiSnSb and PtBiSnSb IMCs retained 70.2% and 62.7% of their initial values, respectively, while the Pt/C electrocatalyst only retained 23.1%. The corresponding characterizations demonstrated that the leaching of Bi/Sn/Sb in IMC nanoplates after cycle tests under high potential (>0.8 V) resulted in the decrease in their MOR activities Theoretical calculations show that the presence of Rh atoms improves the electron transfer efficiency in PtRhBiSnSb IMCs, leading to a significant increase in oxidation capability. The anti-poisoning ability is essential for alcohol oxidation catalysts because noble metals are easy to be poisoned by adsorbed intermediates. The introduction of Rh results in a slightly decreased d-band center of the surface Pt site, which suppresses the overbinding of the intermediates. In this report, a CO-free pathway for the MOR was proposed as evidenced by the *in-situ* Fourier transform infrared (FTIR) and attenuated-total-reflection surface-enhanced infrared absorption spectra (SEIRAS). During the reaction, methanol is firstly oxidized to $HCOO^-$ and then to CO_2. The adsorbed CO_2 is desorbed and reacted with OH to form CO_3^{2-}/HCO_3^-. As a result, the obtained PtRhBiSnSb IMC catalyst avoids the usual CO poisoning problem (Fig. 7c). Meanwhile, the authors also reveal that PtRhBiSnSb IMC catalysts exhibit high activity

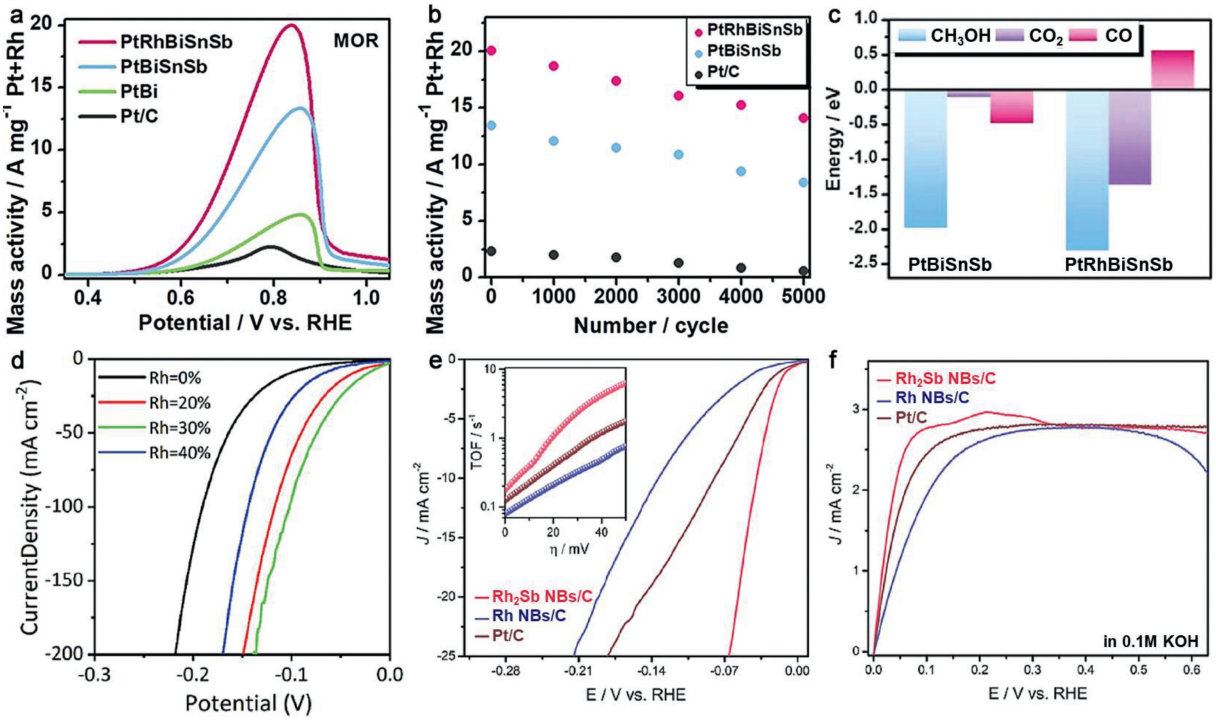

Fig. 7. (a) MOR positive-going polarization curves of different catalysts captured at a scan rate of 50 mV/s. (b) The changes of mass activities for different catalysts before and after cycle tests. (c) The adsorption energy comparison of CO, CO_2, and CH_3OH on high-entropy PtRhBiSnSb IMC nanoplates and PtBiSnSb nanoplates. Reproduced with permission [69]. Copyright 2022, Wiley-VCH. (d) The linear sweep voltammetry curves of $Ir_{1-x}Rh_xSb$ with various x values, in which the sample with $x = 30\%$ shows the best performance. Reproduced with permission [71]. Copyright 2022, Wiley-VCH. (e) HER polarization curves of Pt/C, Rh NBs/C, and Rh_2Sb NBs/C in Ar-saturated 0.1 mol/L KOH (scan rate: 5 mV/s). Inset: TOF values of different electrocatalysts. (f) HOR polarization curves of Pt/C, Rh NBs/C, and Rh_2Sb NBs/C in H_2-saturated 0.1 mol/L KOH (scan rate: 5 mV/s; rotating speed: 1600 rpm). Reproduced with permission [64]. Copyright 2021, Wiley-VCH.

towards the electrooxidation of glycerol and ethanol in alkaline electrolytes.

Compared with MOR, the ethanol oxidation reaction (EOR) is more complicated but more important since methanol is a toxic alcohol, while ethanol is nontoxic and possesses higher energy density [101–103]. However, the reaction kinetics of EOR is more sluggish than MOR because it involves the dehydrogenation of ethanol, as well as the necessity to break the C–C bond to achieve full oxidation. The weak activity of most anode electrocatalysts for C–C cleavage is the main obstacle to the widespread application of DEFCs. Some recent studies showed that the addition of Rh to Pt- or Pd- based catalysts not only improves the C–C cleavage in EOR but also enhances the resistance to poisoning species (mainly CO) [104,105]. Taking PtRh-SnO_2/C as an example, the electron transfer from Rh to Pt results in moderate bonding between Rh and ethanol, intermediates, and products, facilitating the splitting of the C–C bond [106]. Some Rh-based IMCs were successively prepared and demonstrated as effective catalysts for EOR [69,99]. Liu and co-workers reported the synthesis of RhBi-Bi_2O_3 with excellent EOR catalytic activities [98]. The EOR mass activity of RhBi-Bi_2O_3 is about 2.5 times and 80 times higher than those of commercial Pd/C and pristine Rh catalysts, respectively. The weaker adsorption of toxic intermediates caused by the addition of Bi to downshift the d-band center of Rh and the enriched supply of oxygenated species by freestanding Bi_2O_3 are the two reasons for the increased catalytic activity.

3.5. Hydrogen evolution and hydrogen oxidation

Hydrogen is a promising alternative to traditional fossil fuels [107,108]. Recently, Rh-based IMs have emerged as promising electrocatalysts for hydrogen production and utilization, including hydrogen evolution reaction (HER) and hydrogen oxidation reaction (HOR) [22,64,71,109].

There are two elementary steps in the HER process, *i.e.*, the adsorption of hydrogen ($H^+ + e^- \rightarrow H^*$) and the release of molecular hydrogen *via* either the Tafel ($2H^* \rightarrow H_2$) or the Heyrovsky ($H^* + H^+ + e^- \rightarrow H_2$) mechanism [110–113]. Thus, to achieve the dynamic equilibrium between proton uptake and hydrogen release, the Gibbs free energy of H adsorption (ΔG_H) must be close to zero for an idea HER catalyst, which implies the H adsorption should be neither too weak nor strong [114–118]. The adsorption energy can be manipulated by turning the compositions in the IMC-based catalysts. For example, ternary $Ir_{1-x}Rh_xSb$ IMCs with different compositions were prepared by the arc-melting method [71]. The $Ir_{0.7}Rh_{0.3}Sb$ exhibits excellent HER activity with an overpotential of 22 mV at 10 mA/cm^2 in 0.5 mol/L H_2SO_4, which is superior to that of commercial Pt/C (Fig. 7d). The potential did not increase obviously for more than 55 h. And the structure of $Ir_{1-x}Rh_xSb$ could be well maintained after the long-term stability test. According to DFT calculations, the exposed Sb termination in IrSb IMC has insufficient H adsorption capacity, but the exposed metallic Ir site has strong H adsorption. The incorporation of Rh into IrSb alleviates the adverse thermodynamic limitation of both Sb and Ir sites, leading to a moderate H adsorption ability. Rh-based IMCs also show excellent HER and HOR performance in alkaline electrolytes. Zhang *et al.* prepared the branched Rh_2Sb IMCs with atomically isolated Rh sites [64]. Benefited from the unique structure, Rh_2Sb IMCs exhibit excellent HER performance with a low overpotential of 39.5 mV at 10 mA/cm^2 (Fig. 7e). Meanwhile, Rh_2Sb IMCs, in contrast to Rh/C and commercial Pt/C, exhibits substantially superior intrinsic activity and much faster kinetics for HOR (Fig. 7f).

4. Summary and outlook

In this review, we summarize the preparation strategies and synthetic protocols of Rh-based IMC nanocrystals, in which the wet chemical method and thermal annealing method are highlighted. For the formation of an atomic ordered structure, the key is the precise control of the disorder-to-order transition. Based on the theories of thermodynamic control and kinetic control, the composition and ordered structure could be well-tuned according to the phase diagrams. In the main text, the ingenious preparation cases are emphasized. Subsequently, the applications of Rh-based IMCs in a series of catalytic reactions, including semihydrogenation of acetylene, hydroformylation, chemoselective hydrogenation of nitroarenes, electrocatalytic alcohol oxidation, HER, and HOR, are discussed. Meanwhile, the critical roles of ordered IMC structure in improving catalytic performance are illustrated. Many achievements have been made in this area. However, the mechanisms related to the formation of Rh-based IMCs and their catalytic properties are still not explicated clearly. Herein, we will put forward the following points to be explored in the near future:

(1) Till now, the preparation of bulk Rh-based IMCs can be achieved according to the guidance of the phase diagram [43,52]. However, for synthesizing Rh-based IMC nanomaterials, it is still a great challenge to realize the precise control of the vital parameters simultaneously, including size, morphology, crystal structure, and uniformity, because of the melting-point depression phenomenon. So new theories are urgently needed, especially for extending the applicability of phase diagrams. Meanwhile, the thermodynamic and kinetic controls of the nucleation and growth processes should be carried out to guide the preparation of Rh-based IMC nanomaterials.

(2) The disorder-to-order transition is vital for forming an ordered structure. However, the characterizations of the transition process and structural evolution are challenging because of the accuracy and precision limitation of the current characterization equipment at the atomic level [119,120]. Therefore, *in-situ* characterization techniques are needed to develop to reveal the atom diffusion behaviors during the phase transition from disordered solid solution to ordered IMC nanomaterials at high temperature, metal precursors to ordered IMC nanomaterials under reductive atmosphere, *etc*.

(3) Given the wide applications of Rh-based IMCs, the future market demand is expected to be significant. Despite the substantial advances in the fabrication of Rh-based IMCs, the prepared products are typically on a gram or even milligram scale, falling far away from the requirements of industrial-scale production. Several challenges hinder the industrialization of Rh-based IMCs. Firstly, current synthetic methods (*i.e*., impregnation method, wet-chemical method) face major challenges with scaling. Synthetic conditions can be precisely controlled when catalysts are fabricated on a laboratory scale, resulting in Rh-based IMCs with excellent particle dispersion. However, when the synthesis scale is expanded, non-uniform mass and heat transfer effects inevitably occur, leading to local over-concentration and the agglomeration of metallic species. Secondly, the fabrication cost of Rh-based IMCs remains prohibitively high, owing to the cumbersome experimental procedures, expensive equipment requirements, and low production efficiency. Hence, it is imperative to develop simpler, more economical, and readily scalable fabrication methods for the large-scale synthesis of IMCs.

(4) The stability and anti-poisoning property are important for long-term usage in catalytic reactions under harsh reaction conditions. So, understanding the mechanisms of performance degradation is essential. And based on this, the durability of the Rh-based IMCs could be further promoted.

(5) The understanding of the quantitative structure-activity relationship of Rh-based IMCs in various catalytic reactions is unclear. For solid solutions, the disordered atomic arrangement is not suitable for revealing the active sites; on the contrary, the ordered structures of IMCs provide ideal models [121]. More efforts should be dedicated to the characterization of key intermediates in reactions and dynamic structural evolution of catalysts by employing the *in-situ* XPS, *in-situ* FT-IR and *in-situ* Raman spectroscopy, and so on [122,123]. Meanwhile, with the assistance of theoretical calculations, the scientists could get more convincing evidence about the relationship among the atomic structure, electronic structure, and catalytic performance [124].

It is envisaged that the high performance and low-cost Rh-based IMC nanomaterials can be obtained for catalysis based on the rational design of the ordered structure, rigorous preparation protocols, together with the advanced characterization techniques.

Declaration of competing interest

The authors declare that they have no known competing financial interests or personal relationships that could have appeared to influence the work reported in this paper.

Acknowledgments

This work was financially supported by the National Natural Science Foundation of China (Nos. 92061119, 52102286), Guangdong Basic and Applied Basic Research Foundation (No. 2022A1515140051), the Beijing NOVA Program (Nos. Z201100006820066, 20220484172), Beijing Information Science & Technology University, and Key Laboratory Fund Project (No. 202105509).

References

[1] S. Seetharaman, Treatise On Process Metallurgy, Elsevier, Boston, 2014.
[2] F.K. Crundwell, M.S. Moats, V. Ramachandran, et al., Extractive Metallurgy of Nickel, Cobalt and Platinum Group Metals, Elsevier, Oxford, 2011.
[3] L. Luo, H. Li, Y. Peng, et al., ChemNanoMat 4 (2018) 451–466.
[4] M. Chen, G. Gupta, C.W. Ordonez, et al., J. Am. Chem. Soc. 143 (2021) 20907–20915.
[5] S. Furukawa, T. Komatsu, ACS Catal. 6 (2016) 2121–2125.
[6] S. Furukawa, Y. Yoshida, T. Komatsu, ACS Catal. 4 (2014) 1441–1450.
[7] G. Beamson, A.J. Papworth, C. Philipps, et al., J. Catal. 269 (2010) 93–102.
[8] G. Moos, M. Emondts, A. Bordet, et al., Angew. Chem. Int. Ed. 59 (2020) 11977–11983.
[9] G. Beamson, A.J. Papworth, C. Philipps, et al., J. Catal. 278 (2011) 228–238.
[10] H. Tian, J. Zhou, Y. Li, et al., ChemCatChem 11 (2019) 5543–5552.
[11] L. Wang, W. Zhang, S. Wang, et al., Nat. Commun. 7 (2016) 14036.
[12] J. Ge, P. Yin, Y. Chen, et al., Adv. Mater. 33 (2021) 2006711.
[13] Y.Q. Kang, Q. Xue, Y. Zhao, et al., Small 14 (2018) 1801239.
[14] S. Xing, Z. Liu, Q. Xue, et al., Appl. Catal. B 259 (2019) 118082.
[15] X. Zhao, H. Zhao, J. Sun, et al., Chin. Chem. Lett. 31 (2020) 1782–1786.
[16] Z. Wang, H. Zhang, S. Liu, et al., Chem. Commun. 56 (2020) 13595–13598.
[17] J.Y. Zhu, S. Chen, Q. Xue, et al., Appl. Catal. B 264 (2020) 118520.
[18] B. Qiao, T. Yang, S. Shi, et al., Small 17 (2021) 2006534.
[19] S.H. Han, H.M. Liu, P. Chen, et al., Adv. Energy Mater. 8 (2018) 1801326.
[20] Y. Yang, H. Huang, C. Yang, et al., ACS Appl. Energy Mater. 4 (2021) 376–383.
[21] X. Fu, Z. Zhao, C. Wan, et al., Nano Res. 12 (2019) 211–215.
[22] H. Zhang, S. Liu, P. Tian, et al., Chem. Eng. J. 435 (2022) 134798.
[23] Q. Wang, M. Ming, S. Niu, et al., Adv. Energy Mater. 8 (2018) 1801698.
[24] F. Luo, L. Guo, Y. Xie, et al., J. Mater. Chem. A 8 (2020) 12378–12384.
[25] Y. Cheng, S. Lu, F. Liao, et al., Adv. Funct. Mater. 27 (2017) 1700359.
[26] J. Liu, W. Niu, G. Liu, et al., J. Am. Chem. Soc. 143 (2021) 4387–4396.
[27] Z. Zhang, G. Liu, X. Cui, et al., Sci. Adv. 7 (2021) eabd6647.
[28] Z. Duan, K. Deng, C. Li, et al., Chem. Eng. J. 428 (2022) 132646.
[29] M. Datler, I. Bespalov, S. Buhr, et al., Catal. Lett. 146 (2016) 1867–1874.
[30] H. Wang, H.D. Abruña, ACS Catal. 9 (2019) 5057–5062.
[31] M.K. Kundu, R. Mishra, T. Bhowmik, et al., J. Mater. Chem. A 6 (2018) 23531–23541.

[32] R.T. Hannagan, G. Giannakakis, R. Réocreux, et al., Science 372 (2021) 1444–1447.
[33] S. García, L. Zhang, G.W. Piburn, et al., ACS Nano 8 (2014) 11512–11521.
[34] A.K. Singh, Q. Xu, ChemCatChem 5 (2013) 652–676.
[35] Y. Sheng, Y. Liu, Y. Yin, et al., Chem. Eng. J. 452 (2023) 139448.
[36] W. Zhang, L. Wang, H. Liu, et al., Nano Lett. 17 (2017) 788–793.
[37] Y. Nakaya, S. Furukawa, Chem. Rev. (2022), doi:10.1021/acs.chemrev.1022c00356.
[38] M. Zhou, C. Li, J. Fang, Chem. Rev. 121 (2021) 736–795.
[39] P. Liu, J.K. Nørskov, Phys. Chem. Chem. Phys. 3 (2001) 3814–3818.
[40] D. Wang, Q. Peng, Y. Li, Nano Res. 3 (2010) 574–580.
[41] S. Furukawa, T. Komatsu, ACS Catal. 7 (2017) 735–765.
[42] W. Xiao, W. Lei, M. Gong, et al., ACS Catal. 8 (2018) 3237–3256.
[43] Y. Yan, J.S. Du, K.D. Gilroy, et al., Adv. Mater. 29 (2017) 1605997.
[44] J.T.L. Gamler, H.M. Ashberry, S.E. Skrabalak, et al., Adv. Mater. 30 (2018) 1801563.
[45] S. Furukawa, K. Takahashi, T. Komatsu, Chem. Sci. 7 (2016) 4476–4484.
[46] M. Miyazaki, S. Furukawa, T. Komatsu, J. Am. Chem. Soc. 139 (2017) 18231–18239.
[47] Z. Wu, E. Borretto, J. Medlock, et al., ChemCatChem 6 (2014) 2762–2783.
[48] P. Yin, M.X. Chen, M. Zuo, et al., ACS Mater. Lett. 4 (2022) 1350–1357.
[49] Y. Yang, M. Wei, J. Mater. Chem. A 8 (2020) 2207–2221.
[50] J. Li, S. Sun, Acc. Chem. Res. 52 (2019) 2015–2025.
[51] C.L. Yang, L.N. Wang, P. Yin, et al., Science 374 (2021) 459–464.
[52] W.J. Zeng, C. Wang, Q.Q. Yan, et al., Nat. Commun. 13 (2022) 7654.
[53] T.W. Song, C. Xu, Z.T. Sheng, et al., Nat. Commun. 13 (2022) 6521.
[54] S. Kuang, M. Li, X. Chen, et al., Chin. Chem. Lett. 33 (2022) 108013.
[55] Y. Yuan, Z. Yang, W. Lai, et al., Chem. Eur. J. 27 (2021) 16564–16580.
[56] X. Li, J. Zhao, D. Su, Small Struct. 2 (2021) 2100011.
[57] K.D. Gilroy, A. Ruditskiy, H.C. Peng, et al., Chem. Rev. 116 (2016) 10414–10472.
[58] T.S. Rodrigues, M. Zhao, T.H. Yang, et al., Chem. Eur. J. 24 (2018) 16944–16963.
[59] A. Ruditskiy, H.C. Peng, Y. Xia, Annu. Rev. Chem. Biomol. Eng. 7 (2016) 327–348.
[60] Y. Yao, S. Hu, W. Chen, et al., Nat. Catal. 2 (2019) 304–313.
[61] A.L. Wang, L. Zhu, Q. Yun, et al., Small 16 (2020) 2003782.
[62] W.M. Haynes, D.R. Lide, T.J. Bruno, CRC Handbook of Chemistry and Physics, CRC Press, 2016.
[63] Y. Yao, X.K. Gu, D. He, et al., J. Am. Chem. Soc. 141 (2019) 19964–19968.
[64] Y. Zhang, G. Li, Z. Zhao, et al., Adv. Mater. 33 (2021) e2105049.
[65] Y.J. Zhu, F. Chen, Chem. Rev. 114 (2014) 6462–6555.
[66] D.P. Dutta, Microwave-Assisted Synthesis of Inorganic Nanomaterials, Handbook on Synthesis Strategies For Advanced Materials: Volume-I: Techniques and Fundamentals, Springer, Singapore, 2021.
[67] D. Köhler, M. Heise, A.I. Baranov, et al., Chem. Mater. 24 (2012) 1639–1644.
[68] J. Teichert, M. Heise, J.H. Chang, et al., Eur. J. Inorg. Chem. 2017 (2017) 4930–4938.
[69] W. Chen, S. Luo, M. Sun, et al., Adv. Mater. 34 (2022) e2206276.
[70] M. Cui, C. Yang, S. Hwang, et al., Sci. Adv. 8 (2022) eabm4322.
[71] Z. Lin, B. Xiao, M. Huang, et al., Adv. Energy Mater. 12 (2022) 2200855.
[72] S. Furukawa, A. Yokoyama, T. Komatsu, ACS Catal. 4 (2014) 3581–3585.
[73] S. Furukawa, K. Ochi, H. Luo, et al., ChemCatChem 7 (2015) 3472–3479.
[74] T. Komatsu, S. Furukawa, J. Japan Pet. Inst. 63 (2020) 336–344.
[75] S. Furukawa, T. Komatsu, K.I. Shimizu, J. Mater. Chem. A 8 (2020) 15620–15645.
[76] X. Ji, K.T. Lee, R. Holden, et al., Nat. Chem. 2 (2010) 286–293.
[77] W. Li, J. Liu, D. Zhao, Nat. Rev. Mater. 1 (2016) 16023.
[78] L. Rößner, M. Armbrüster, ACS Catal. 9 (2019) 2018–2062.
[79] J.K. Nørskov, T. Bligaard, B. Hvolbæk, et al., Chem. Soc. Rev. 37 (2008) 2163–2171.
[80] V.S. Marakatti, S.C. Peter, Prog. Solid State Chem. 52 (2018) 1–30.
[81] Q. Feng, S. Zhao, Y. Wang, et al., J. Am. Chem. Soc. 139 (2017) 7294–7301.
[82] J. Zhang, W. Xu, L. Xu, et al., Chem. Mater. 30 (2018) 6338–6345.
[83] A. Dasgupta, R.M. Rioux, Catal. Today 330 (2019) 2–15.
[84] R.V. Maligal-Ganesh, Y. Pei, C. Xiao, et al., ChemCatChem 12 (2020) 3022–3029.
[85] B. Breit, Acc. Chem. Res. 36 (2003) 264–275.
[86] R. Franke, D. Selent, A. Börner, Chem. Rev. 112 (2012) 5675–5732.
[87] P. Dingwall, J.A. Fuentes, L.E. Crawford, et al., J. Am. Chem. Soc. 139 (2017) 15921–15932.
[88] J. Pospech, I. Fleischer, R. Franke, et al., Angew. Chem. Int. Ed. 52 (2013) 2852–2872.
[89] X.L. Zheng, C.Y. Zheng, F.D. Zhou, et al., Chin. Chem. Lett. 27 (2016) 678–680.
[90] H.K. Kadam, S.G. Tilve, RSC Adv. 5 (2015) 83391–83407.
[91] T. Aditya, A. Pal, T. Pal, Chem. Commun. 51 (2015) 9410–9431.
[92] S. Cai, H. Duan, H. Rong, et al., ACS Catal. 3 (2013) 608–612.
[93] Z. Xia, X. Zhang, H. Sun, et al., Nano Energy 65 (2019) 104048.
[94] Y. Liu, Z. Yu, J. Chen, et al., Chin. Chem. Lett. 33 (2022) 1817–1830.
[95] D.M. Fadzillah, S.K. Kamarudin, M.A. Zainoodin, et al., Int. J. Hydrog. Energy 44 (2019) 3031–3054.
[96] Y. Mu, T. Wang, J. Zhang, et al., Electrochem. Energy Rev. 5 (2022) 145–186.
[97] N. Cheng, L. Zhang, K. Doyle-Davis, et al., Electrochem. Energ. Rev. 2 (2019) 539–573.
[98] Y. Liu, B. Lan, Y. Yang, J. Mater. Chem. A 10 (2022) 20946–20952.
[99] S. Luo, L. Zhang, Y. Liao, et al., Adv. Mater. 33 (2021) 2008508.
[100] D. Wang, Z. Chen, Y. Wu, et al., SmartMat 4 (2023) e1117.
[101] S. Bai, Y. Xu, K. Cao, et al., Adv. Mater. 33 (2021) 2005767.
[102] T. Kwon, M. Jun, J. Joo, et al., J. Mater. Chem. A 7 (2019) 5090–5110.
[103] M.A. Zeb Gul Sial, M.A. Ud Din, X. Wang, Chem. Soc. Rev. 47 (2018) 6175–6200.
[104] D.B. Huang, P.L. He, Q. Yuan, et al., Chem. Asian J. 10 (2015) 608–613.
[105] N.S. Marinkovic, M. Li, R.R. Adzic, Top. Curr. Chem. 377 (2019) 11.
[106] A. Kowal, M. Li, M. Shao, et al., Nat. Mater. 8 (2009) 325–330.
[107] N. Sazali, Int. J. Hydrog. Energy 45 (2020) 18753–18771.
[108] X. Li, Z. Wang, Y. Tian, et al., Chin. Chem. Lett. 33 (2022) 107812.
[109] A. Jiang, J. Chen, S. Liu, et al., ACS Appl. Nano Mater. 4 (2021) 13716–13723.
[110] B. You, Y. Sun, Acc. Chem. Res. 51 (2018) 1571–1580.
[111] Q. Lu, Y. Yu, Q. Ma, et al., Adv. Mater. 28 (2016) 1917–1933.
[112] S. Han, Q. Yun, S. Tu, et al., J. Mater. Chem. A 7 (2019) 24691–24714.
[113] L. Zhang, K. Doyle-Davis, X. Sun, Energy Environ. Sci. 12 (2019) 492–517.
[114] Y. Zheng, Y. Jiao, A. Vasileff, et al., Angew. Chem. Int. Ed. 57 (2018) 7568–7579.
[115] M. Zeng, Y. Li, J. Mater. Chem. A 3 (2015) 14942–14962.
[116] Z. Li, Y. Yue, J. Peng, et al., Chin. Chem. Lett. 34 (2023) 107119.
[117] Z. Luo, J. Li, Y. Li, et al., Adv. Energy Mater. 12 (2022) 2103823.
[118] L. Zhang, R. Si, H. Liu, et al., Nat. Commun. 10 (2019) 4936.
[119] Y. Xiong, Y. Yang, H. Joress, et al., Proc. Natl. Acad. Sci. U. S. A. 116 (2019) 1974–1983.
[120] H. Chen, Y. Yu, H.L. Xin, et al., Chem. Mater. 25 (2013) 1436–1442.
[121] H. Zhang, P. Shi, X. Ma, et al., Adv. Energy Mater. 13 (2023) 2202703.
[122] H. Zhang, Y. Li, C. Cheng, et al., Angew. Chem. Int. Ed. 62 (2022) e202213351.
[123] D. Bagchi, J. Raj, A.K. Singh, et al., Adv. Mater. 34 (2022) 2109426.
[124] P. Wu, J. Zaffran, D. Xu, et al., J. Phys. Chem. C 124 (2020) 15977–15987.